Summer 2018

Integrated geophysical methods to characterize subsidence in Butte, Montana, U.S.A.

Kristen Prudhomme
Montana Tech

Recommended Citation

Prudhomme, Kristen, "Integrated geophysical methods to characterize subsidence in Butte, Montana, U.S.A." (2018). *Graduate Theses & Non-Theses*. 179.
https://digitalcommons.mtech.edu/grad_rsch/179

Integrated geophysical methods to characterize subsidence in Butte, Montana, U.S.A.

Kristen D. Prudhomme[1], Mohamed A. Khalil[1], Glenn D. Shaw[2], Marvin A. Speece[1], Katherine R. Zodrow[3] and Tom Malloy[4]

[1]Montana Tech, Department of Geophysical Engineering,
Butte, MT, 59701
Email: kprudhomme@mtech.edu

[2]Montana Tech, Department of Geological Engineering,
Butte, MT, 59701

[3]Montana Tech, Department of Environmental Engineering,
Butte, MT, 59701

[4]City and County of Butte-Silver Bow,
Butte, MT, 59701

ABSTRACT

Geophysical investigations, designed to characterize unique subsidence features of unknown natural origin, provide imaging analysis of potential causes of subsidence. Recent subsidence in the alluvial plain in Butte, Montana is unrelated to historic mining in the area. This study aims to utilize a combined application of shallow electrical resistivity tomography (ERT), self-potential (SP), and frequency-domain electromagnetic (FDEM) methods in order to develop a better understanding of the particular set of hydrogeological and environmental conditions that contribute to this unique phenomena. Geophysical measurements provide lateral and vertical variations of electrical resistivity in the subsurface to a depth of 10 m while also contouring the streaming potential in each site to help characterize the site-specific groundwater flow components. Least-square inversion resistivity models and conductivity from electromagnetic data are compared to known well lithologic information to identify general variations of sediments with depth as well as delineate the extent of the known subsidence features. Site investigations indicate that the subsidence features in basin fill sediments are spatially associated with electrical and electromagnetic signatures of water seepage and sharp contacts between resistive and conductive sediment layers. ERT results showed a circular resistive anomaly in place of known subsidence locations and delineated lithologic heterogeneity in each site, suggesting a clay contact at shallow depth. The FDEM results complemented ERT and further characterized the depth and thickness of the clay lens. The SP results indicated surficial seepage associated with subsidence locations. This work sets a baseline site

characterization and analysis on the origin of these subsidence features, where the subsidence is expected to be associated with volumetric changes in clay and porous media during surficial seepage.

Introduction

Subsidence hazards depend on a variety of natural and man-made conditions and are able to dramatically alter local and regional hydrogeologic systems. Subsidence features associated with man-made structures and voids are common in areas with mining and drilling operations, where buried artifacts, dewatering and extraction methods, and time are relative factors in considering mining activity associated with subsidence (Bozeman, M.T., 2002). Other subsidence features can occur naturally from karstification effects, over pumping of an aquifer, swelling of soils due to an increase of surface water infiltration, seismic and non-seismic liquefaction, frost action, and artificial recharge (Soupios et al, 2007; Bozeman, M.T., 2002, Zhang et al., 2015, Tuttle, 2001, Clark and Holzer, 1993). In order to remediate subsidence conditions, site-specific characterizations are implemented to determine the extent and source of vertical displacement of material in the ground surface.

The city of Butte, Montana is a well-known superfund site with a rich history of world-class mining of copper and silver, in which the land surface and structure has been dramatically altered. Further, the original hydrologeological system has been altered by the contribution of the Berkeley Pit's 200 billion gallon lake of acid mine water (pH 4-4.1) (http://mbmggwic.mtech.edu/), which has jeopardized the groundwater flow and quality in Silver Bow Creek. This has created a complex hydrogeological setting and affected the underlying shallow alluvial aquifer (Bozeman, M.T., 2002). Residents of Butte have experienced the long-term repercussions of mining activity from the 1800's through today, particularly where old discovery and production mine shafts have been linked to occurrences of subsidence throughout urban development (Bozeman, M.T., 2002). Most mine shafts have been documented, and subsidence features near these mine shafts have been determined to originate from mining activity.

The subsidence features examined in this study suggest a unique condition to the Butte area. The features were reported during the last 10 years in a suburban area south of the Berkeley Pit (Figure 1). However, we note that more subsidence features have not been reported to the city and have potentially opened up earlier than 2008. The features are characterized by circular depressions suddenly forming in residential sites. These hazards are causing harm to structures in these sites, expressed as cracking in the concrete sidewalks and brick buildings. Due to the increasing danger to residents, the City and County of Butte Silver Bow is investigating the cause of subsidence in this region.

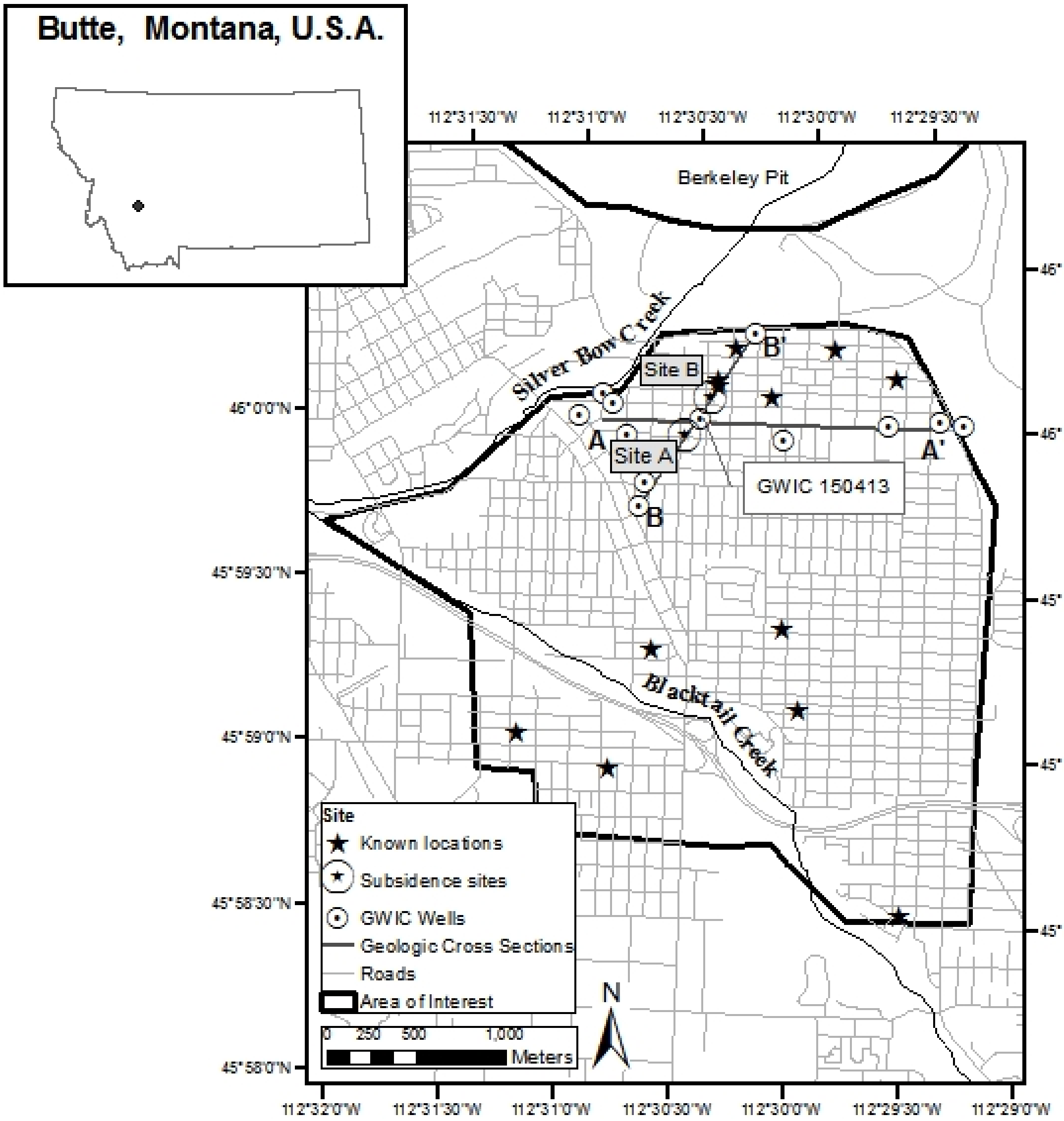

Figure 1. The hazards of unknown origin in Butte, MT. Sites with geophysical investigation are shown in circles. The density of features increase above the geological cross-sectional line A-A'. Well locations are supplied through GWIC data, and stream location is generalized from the Montana State Library database, with Silver Bow Creek reflecting its historic path.

The conditions for karstification, seismic-induced liquefaction, over pumping, and frost heave are not considered to be likely causes of subsidence in the region. Natural causes of subsidence applicable to the study area include non-seismic induced liquefaction, artificial recharge, and swelling of soils due to surfical seepage. Each of these mechanisms can be explained by one or a combination of the common processes behind subsidence, as listed in de Glopper and Ritzema, 1994: 1) compression-compaction, 2) consolidation, 3) shrinkage, 4) and oxidation. Non-seismic liquefaction, as summarized in Holzer and

Clark, 1993, is a soft-sediment deformation in which associated liquefaction features would form bowl-shaped pockets, dikes, and sand blows along a large fissure zone, allowing for hydraulic connectivity between all associated collapse features (Bezerra, et al., 2005, Wolf et al., 1998, Obermeier, 1996, Holzer and Clark, 1993)). Artificial recharge pertains to the visco-plastic deformation of an aquifer or aquitard, which is a lagging process occurring after pumping of an aquifer has ceased, as explained in Zhang et al., 2015. The swelling and shrinking of soils can occur when surface water infiltrates the subsurface and swelling clays are present, causing clay dehydration that attributes to volume reduction (Bull, 1964, Liu and Li, 2005, Stumpf 2013). The process of hydrocompaction, a soft sediment deformation in sandy to silty sediment, is dependent on surface water infiltration and will create large void spaces within the sandy material (Zisman and West, 2015). Both clay dehydration and hydrocompaction are considered under the category of swelling soils. Detailed analysis on the soil mechanics associated with each subsidence feature is not addressed in this study; however, based on geological and geophysical evidence, conclusions can be made on the possible driving mechanisms behind the subsidence in the area of interest.

Geophysical techniques can be used to image subsidence features, as well as buried artifacts from human activity. Mine shafts and man-made structures will be expressed as an anomaly with geometric regularity (Soupios et al, 2007), with mine shafts in particular being expressed as resistive dike-like features (Reynolds, 2011). In the case study by Soupios et al, 2007, electrical resistivity tomography (ERT) and frequency domain electromagnetics (FDEM), were utilized to identify the sources of hazards with cavities in heterogeneous geologic conditions. Areas with clay were more susceptible to subsidence in changing environmental conditions (Soupios et al, 2007). This provides a basis for understanding the association of clay with known subsidence hazards detected through geophysical investigations. In a study done by Doolittle et al, 2002, liquefaction features in alluvial soils associated with clay content are mapped through geophysical methods, where high-resistivity coarse grained responses were anomalous features within fine grained material. Liquefaction features were associated with heterogeneity within facies in channel fill deposits (Doolittle et al., 2002. Wolf et al., 1998). Further, the surface and groundwater conditions of a site are known to be a factor in subsidence occurrences. A study conducted at the Hidden Dam in California by the United States Geological Survey (USGS) utilized ERT and self potential (SP) to identify surficial seepage. SP maps produced negative anomalies in areas with surface water infiltration, while ERT delineated subsurface structural variability that is associated with flow (Burke et al, 2011). In a study by Jardani et al, 2006, the streaming potential anomalies were determined to result from downward infiltration of surface water through loess and into sinkholes, which act as a fluid conduit. The results support the applicability of utilizing SP in the presence of heterogeneous resistivity distribution in a vadose zone (Jardani et al, 2006).

Urban areas pose difficult conditions for geophysical surveying by limiting depth of investigation capabilities as well as imposing noise sources that inhibit the resolution of geophysical data. Electrical and electromagnetic geophysical methods were chosen to optimize near-surface investigation in this urban region. Electrical imaging techniques correspond well with delineating subsidence anomalies throughout resistive media and can provide high signal strength for near-surface investigations (Doolitte et al., 2002, Loke, 2004, Burke et al., 2011). Reported subsidence features in this survey were expected to produce a circular anomaly throughout soil packages, with potential vertical extensions of void space, producing a resistive response (Soupios et al., 2007). Further, the geological material was imaged at depth and we evaluated the heterogeneous packages sand and clay applicability to hydrocompaction or swelling clay layers that interact with surficial seepage in order to promote subsidence.

Site Description

Area of Interest

Mining related hazards are spatially associated with historic mining activity as shown in Figure 2, but the non-mining subsidence features present no obvious association. Fourteen known locations lie within the Silver Bow Creek alluvial basin that have reported occurrences of subsidence since 2008. The area has been developed for over 80 years, and these occurrences suggest that the long-term repercussions of urban development are only recently being realized. The subsidence features in this area have all been reported to open instantaneously, creating circular depressions of an approximate diameter of 0.5-1.5 m and up to 5 m depth. The density of occurrences is observed to increase near the Berkeley pit, shown in the cluster defined in Figure 1.

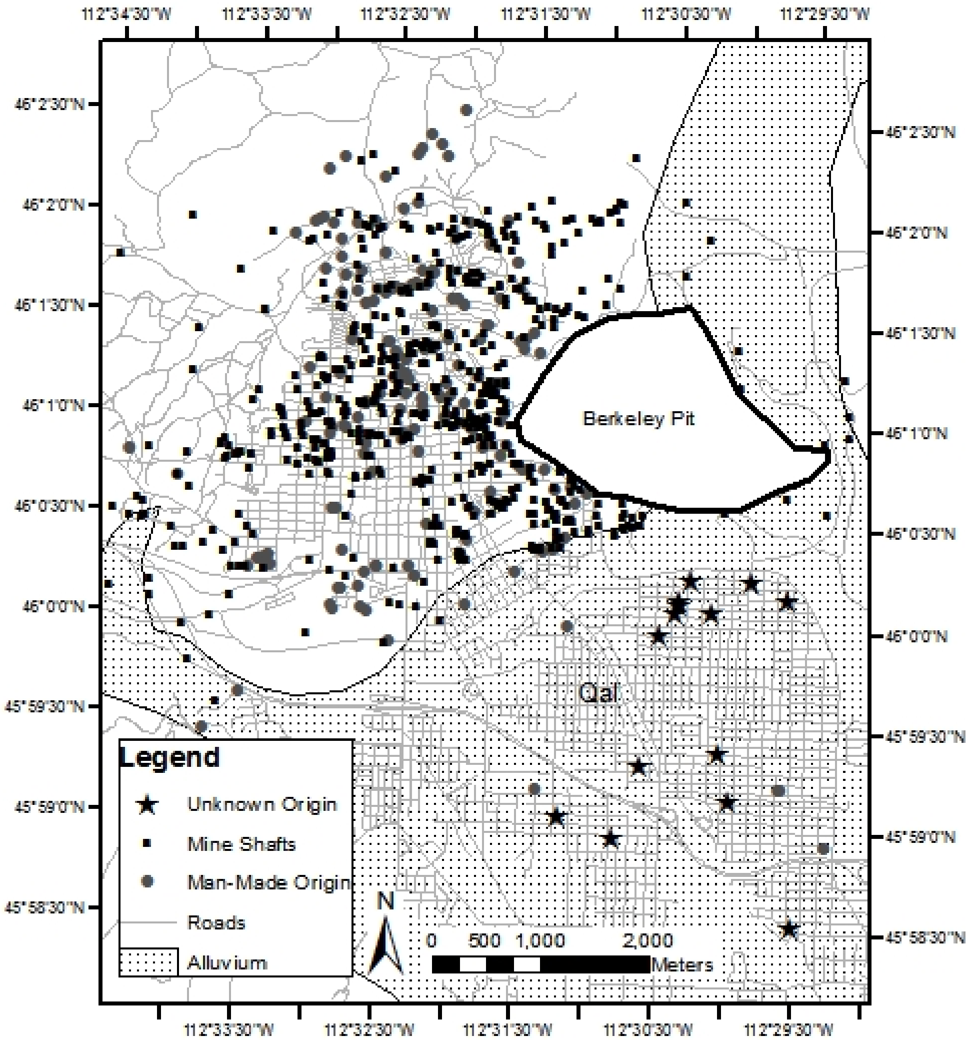

Figure 2 Reported hazards in Butte with spatial relation to mine shafts from historic mining activity. The hazards of unknown origins are isolated and cluster together near to the north, near the pit. All locations were supplied through the City and County of Butte Silver Bow. Hazard sites of interest are shown in triangles.

<u>Geology</u>

The sites of interest lie directly south of Berkeley Pit within a quaternary aged alluvium basin that is bounded by Cretaceous and Tertiary aged igneous strata (Figure 3). The basin lies directly west of the range-bounding normal fault named the Continental Fault, which runs N-S along the East Ridge, and continues eastward, bounded by faults (Zhang, 2000, Newbrough and Gammons, 2002, Gammons, et al., 2006, Mcdonald et al, 2012). The sedimentary basin is expected to be at least 100 m thick, with depositional sequences thickening southward, and is related to Basin and Range type faulting (Houston, 2001). The alluvial deposits at the surface are poorly sorted, unconsolidated silt, sand, pebble, and cobble eroded from the volcanic and granitic rocks of the East Ridge. These deposits are expected to be up to 10 m thick. Within this package, the younger deposits consist of sub-rounded to well-rounded resistant sand, gravel, silt, and clay fluvial debris from modern streams. Older deposits date as late as the Pleistocene era and contain organic floodplain deposits at the surface (McDonald et al, 2012). Deeper sedimentary packages report heaving sand locations around 20 m depth, according to the Montana Ground Water Information Center (GWIC) well lithology information. However, the heaving sands lie below the water table and depth of this investigation. The late Cretaceous and Tertiary igneous rocks where sediments are derived from have come from discrete episodes of volcanic activity with fine-grained andesitic flows (Newbrough and Gammons, 2002, McDonald et al, 2012). The igneous intrusions of the area range from granite to monzonite or diorite, but have similar weathering, soil development, and mechanical properties as granite which is the source for the alluvium in the survey area (Newbrough and Gammons, 2002, United States Department of Agriculture, Natural Resources Conservation Service, 2009). Butte, known for its mining history, has had hydrothermal alterations at depth, but the deposits considered in this study only consider the shallow quaternary aged alluvium.

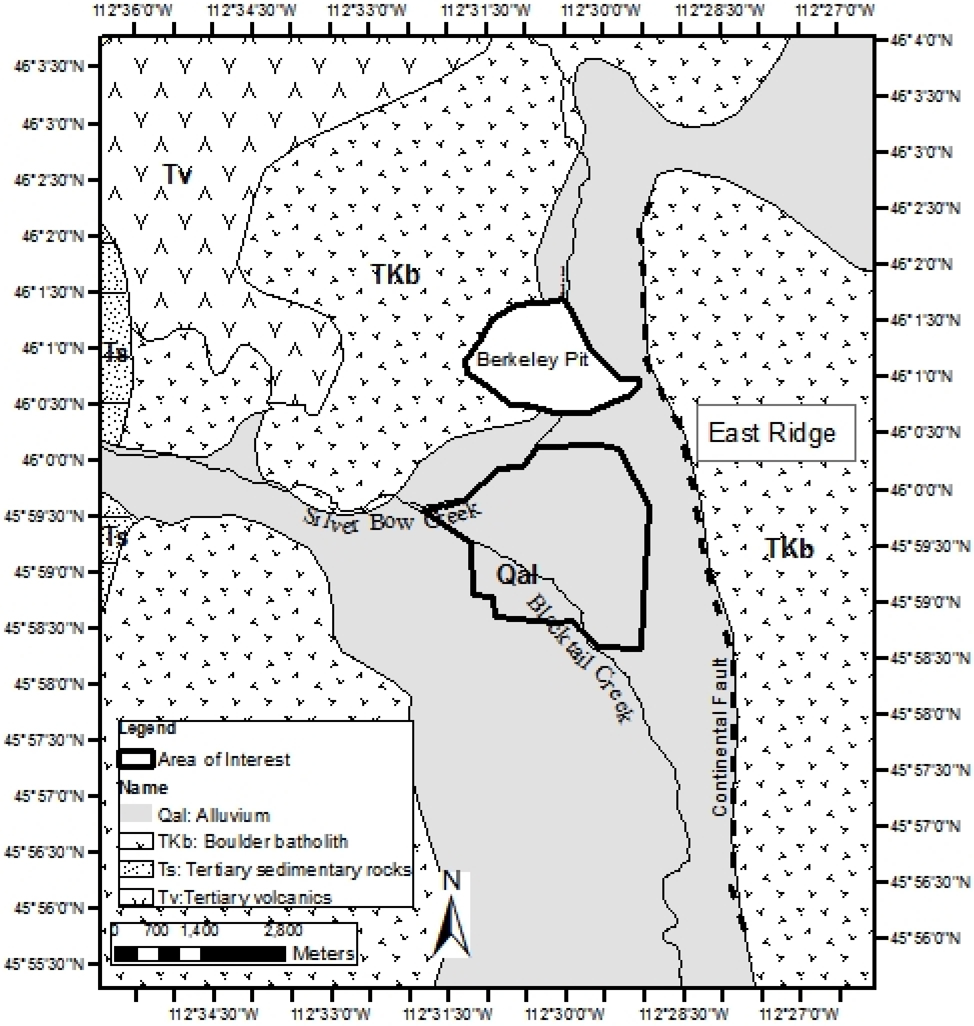

Figure 3 The geologic units for the Butte region, with geologic units supplied by the MBMG.

Hydrogeology

The region consists of three known sand and gravel aquifer units, defined by alternating confining layers of silt and clay. The Butte Priority Soils superfund project, which borders the northwestern boundary of the survey area, defines the shallow aquifer as an unconfined water table bounded below by a continuous clay layer and is estimated to lie at 7-10 m depth based on local well lithology (Tucci and Icopini, 2012,Tucci, 2010, http://data.mbmg.mtech.edu/mapper/mapper.asp?view=Wells&). The basin fill area is characterized hydrogeologically with regional downward gradients. The groundwater flow is directed towards the present-day Silver Bow Creek, Blacktail Creek, and Berkeley pit (Tucci, 2010). The headwaters of Silver Bow Creek are located 10 miles northeast of uptown Butte, where the native hydrogeological system has been altered since the original flow path has been disturbed by the development of Berkeley Pit (Bozeman, M.T., 2002, Gammons, et al, 2006). The creek has historically been the source of recharge for the shallow aquifer, but the creek has also become the transporting source for contaminants from the Parrot Tailings complex (Tucci and Icopini, 2012). However, according to Newbrough and Gammons, 2002, the alluvial sediments west of the Continental Fault have potential to neutralize any contaminated Berkeley Pit water in the presence of seepage. Studies of the Parrot Tailings identified the boundary of the contamination plume, and the sites in this investigation lie outside of the contamination plume (Tucci and Icopini, 2012). Flows have been redirected towards the Berkeley Pit and present day Silver Bow Creek, with pumps being shut off in 1982 with the conclusion of mining activity (Bozeman, M.T., 2002, Tucci and Icopini, 2012). The geophysical investigation in this survey analyzes the hydrogeological conditions within the vadose zone.

Sites of investigation

The sites lie within an eighty year old urban development area with relatively flat terrain. As of 2008, multiple residents within this Silver Bow Creek alluvial basin have reported a circular depression forming instantaneously, with no evidence of a structure or pipe associated with each feature. Some sites have had features re-open after being filled with landscaping material. We have found evidence of settling of structures nearby the subsidence features, damaging concrete sidewalks, brick buildings, and producing damage to asphalt in nearby alley ways. Further, the fourteen known sites are likely to not be the only features in this area. Many witnesses have stated that similar features have opened up within a few blocks of the reported subsidence, which suggests that the conditions for subsidence are not only localized to specific sites but rather an entire geological and hydrogeological system. Out of the fourteen known locations, two were chosen for a detailed and site-specific geophysical investigation due to their accessibility and location within the high-density region of sites, as seen in Figure 1.

Site A. The first site is shown in Figure 4. The site lies southwest of the general cluster, mentioned in Figure 1. The feature was reported to the City and County of Butte Silver Bow in 2012, with the exact date of opening unknown in this investigation. The feature is suggested to be approximately 1 m in diameter and 3.6 m deep; however, these dimensions are estimates made by eyesight from a neighbor. According to witness account, the resident in site A had been excessively watering the back yard for multiple hours per day, and at least five days a week for at least two years prior to the collapse of the soil. Residents removed two trees a few months prior to the collapse of the feature, and the signature of these excavated trees are seen from the surface. The feature has been filled in and the watering has stopped.

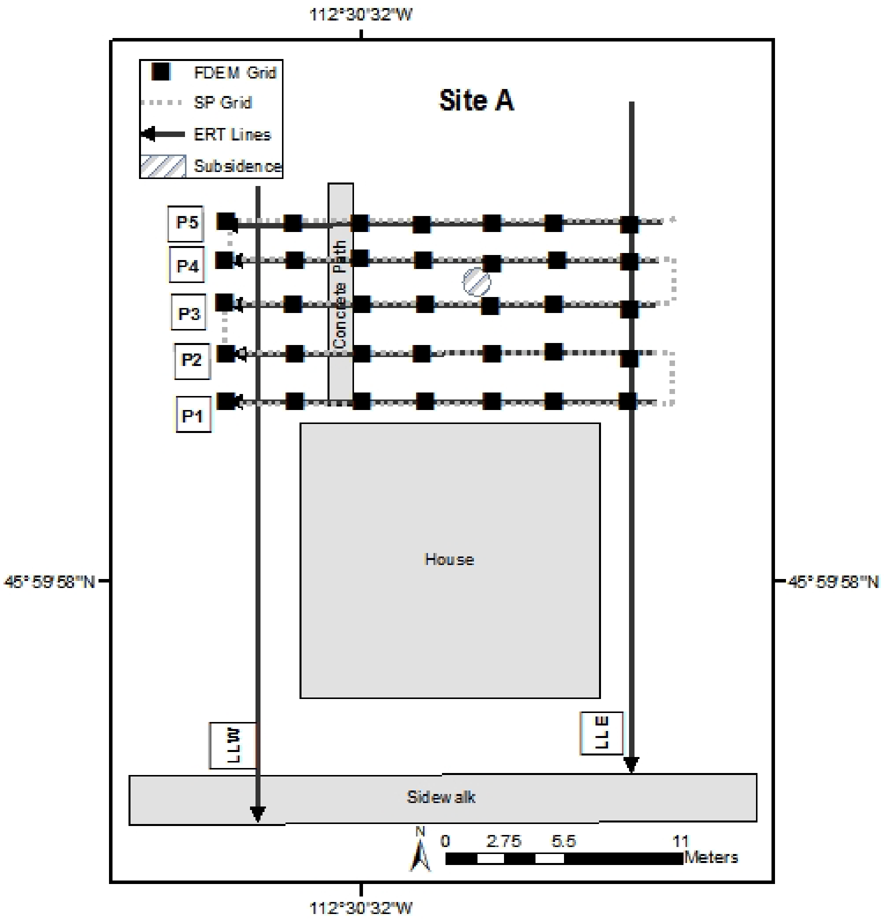

Figure 4. The geophysical survey locations are shown for Site A. A total of seven ERT profiles were collected, with overlying FDEM and SP measurements.

Site B. The second site is shown in Figure 5. The site lies within the general cluster and is closer in proximity to Berkeley Pit than Site A. The feature was reported to the county in 2013, with its original opening occurring in the middle of June. The feature was filled in with landscaping fill, but the ground surface sank again and refilled with concrete. The feature is estimated to be about 0.6 m wide and approximately 2.1 m deep; however, these are estimates based on eyesight from the resident. The resident at this site does not appear to employ excessive watering of the yard, but there is a gardening zone on the southeast edge of the backyard that has been tended for twenty years. The house and the neighboring shed have multiple rain drainage pipes, which are associated with cracks in the sidewalk and shed, suggesting settlement issues associated with surficial seepage like in site A. Three trees on the western side of the property are also located near the cracks in the sidewalk and known subsidence feature. Two other known subsidence features are located within the same residential block as site B, suggesting the geological and hydrogeological conditions present in site B are not only localized to this property.

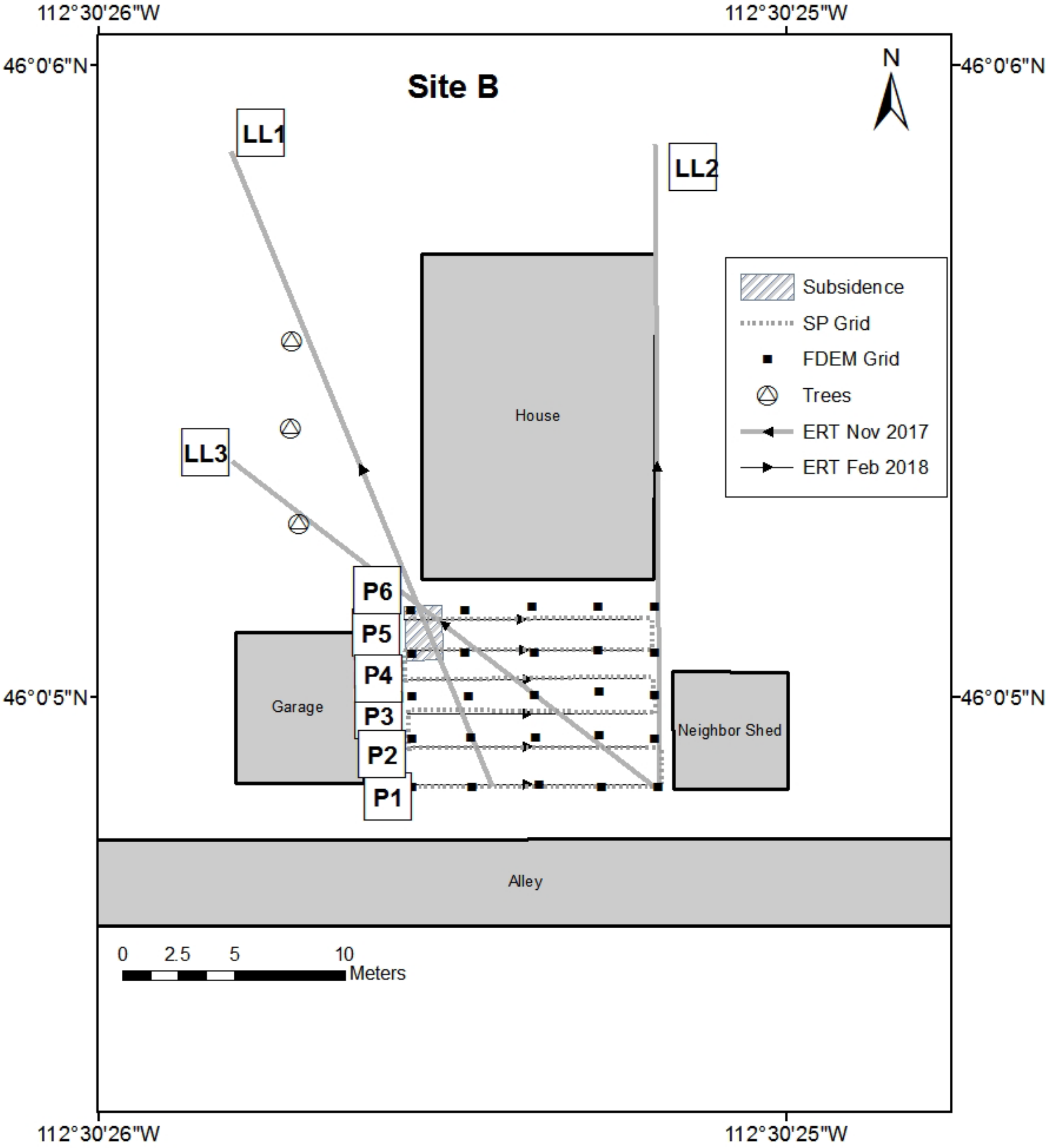

Figure 5 The geophysical survey locations are shown for Site B. A total of nine ERT profiles were collected, with overlying FDEM and SP measurements.

Methodology

We visited five of the fourteen known sites to identify structural damage, factors of causation, availability of area, and applicability of geophysical survey employment. Out of the available sites with known subsidence features, the ideal survey candidate would be able to support a minimum of 30 m in length for ERT surveys to reach a depth of penetration near 6 m, the subsidence feature would lie in penetrable media such as a lawn or dirt, the site could support a 2-D grid of measurements without obstacles or noise sources, and known GWIC wells with lithologic information were nearby. Two sites were chosen to be characterized due to the availability and effectiveness of meeting requirements for baseline survey techniques. ERT, SP, and FDEM were utilized for near-surface sounding due to the high-resolution capabilities in small areas with shallow investigations. Survey designs for both sites aimed to optimize the depth of penetration through ERT profile length as well as measure a 2-D grid for 3-D processing.

ERT is an active method that images subsurface bulk electrical resistivity which provides information about changes in subsurface lithology and groundwater saturation (Burke et al, 2011). During electrolytic conduction, the current flow is associated with movement of ions in groundwater, and resistivity measurements are dependent on the porosity, salinity concentration, and clay content especially within unconsolidated sediments (Loke, 2004). The Wenner array was chosen due to its high signal to noise ratio and ability to detect lithologic structures and vertical discontinuities (Loke, 2004). In the WEnner configuration, the electrode spacing is held constant, and as electrode spacing increases, the depth of investigation will increase and the lateral resolution of bulk resistivity will depend on the spacing between current and potential electrodes (Loke, 2004, Burke, 2011). The goal in this paper is to utilize ERT to delineate geological layers as well as image the filled in subsidence features.

In conjunction with ERT, SP measurements act as a non-intrusive flow sensor and measures the electrical potential caused by subsurface current sources, such as fluid flow in porous media (Burke et al, 2011). Streaming potentials are pH dependent and dominated by the electrical double-layer phenomenon as fluid flow through pore spaces causes an excess drag of the built-up positive charge on mineral grains, expressed as a streaming current density (Revil and Jardani, 2013). In turn the positive self-potentials are attributed to the direction of fluid flow, identifying a decrease in hydraulic head (Burke et al, 2011).

Lastly, FDEM is a close source electromagnetic induction method based on Maxwell's laws. The transmitter and receiver coils are used as horizontal and vertical dipoles to measure a depth of 3 m and 6 m depth, respectively. The receiver coil measures the eddy current generated and the relation between secondary and primary magnetic field is linearly proportional to terrain conductivity under low induction number conditions. FDEM has been used to produce the lateral variation of conductivity values and overcome high contact resistance, which enables a cross-validation with geoelectrical measurements (Soupios et al, 2007). The purpose for this study is to produce lateral variation information of geoelectrical properties of the subsurface.

ERT Measurements

We used a DC resistivity meter Syscal R2 manufactured by IRIS instruments to collect resistivity data. We completed a total of 16 2-D ERT profiles during June 2017-February 2018. A high-resolution ERT grid was designed in each site to correlate multiple parallel 2-D profiles into a 3-D inversion. Each ERT survey utilized the Wenner configuration due to its high sensitivity and signal strength in areas with high background noise. The Wenner array is also sensitive to vertical resolution, in which the subsidence target is expected to have a vertical extent. However, the ERT configuration poses difficulties in overcoming high contact resistance and evaluating lateral changes in resistivity.

ERT Inversion

We performed 2-D and 3-D resistivity inversions of the collected data through the programs Res2DINV and Res3DINV (Loke, 1996). The inversion algorithm, developed by Loke, 1996, is based on the finite element technique, with a robust constrained least-squares method. The robust inversion, or l1-norm, tends to produce a higher resolution with sharp boundaries and more accurately reflect known geology, whereas smoothness-constrained or l2-norm reflects smooth variations in homogenous media such as diffusion boundaries (Loke, 2004). The subsidence features are expected to produce a sharp anomaly within resistive media due to the heterogeneous fill material that has since been emplaced. We applied a half-width spacing model refinement, a technique commonly used with large resistivity variations near the ground surface (Loke, 1996). The reference model value was the average apparent resistivity value from the given dataset. The model was limited to 10 inversions, although some inversions converged at 4-6 iterations. The RMS convergence limit was set to 1%. All parameters were held constant for each 2-D profile and 3-D inversion for both sites.

Error analysis. We manually eliminated bad data points upon the initial inversion with further model outliers eliminated based on generated RMS histogram results, which displays the distribution of percent difference between calculated and measured resistivity values (Loke, 2016). We utilized the L-Curve technique through the Res3DINV program to optimize the dampening factor and evaluate outlier data. RMS values below 2.5% with iterations less than 10 were justified for reasonable model results. The sensitivity value was calculated for each block in the model, displaying the amount of resistivity information contained within the measured data set, with higher values representing a higher reliability of the model result (Loke, 1997). However, the reliability of the model is better represented through the empirical analysis of Depth-of-Investigation index (DOI) for 2-D models and Volume-of-Investigation index (VOI) for 3-D models. The Depth of Investigation Index (DOI) and Volume of Investigation Index (VOI) were calculated by taking a one-sided difference as developed by Oldenburg and Li (1999) in order to quantify the reliability of each 2-D and 3-D ERT, respectively. The equation developed by Oldenburg and Li (1999), shown in Eq (1), incorporates all inverse problem components by generating two models at different reference resistivity's for 2-D inversion, and Eq (2) is used in 3-D inversion VOI calculations.

$$R\,(x,z) = \frac{m_1(x,z) - m_2(x,z)}{m_{1r} - m_{2r}} \qquad (1)$$

$$R\,(x,y,z) = \frac{m_1(x,y,z) - m_2(x,y,z)}{m_{1r} - m_{2r}} \qquad (2)$$

Where R (x,z) or R (x,y,z) denotes the DOI and VOI coefficient, respectively. The variables $m_1(x,z)$ and $m_2(x,z)$ are the model resistivity values corresponding to each background reference resistivity value, m_{1r} and m_{2r}.

The ERT inversion problem is non-unique and poses problems in equivalency. In order to test the reliability of the initial model, two additional models with different reference resistivity values are generated. The DOI value is calculated based on the difference between model resistivity values in order to determine the depth below which the data is no longer sensitive to the physical properties of the subsurface material (Oldenburg and Li, 1999). We applied a one-sided difference DOI and VOI calculation to the models generated in this study, and index values lower than 0.3 are accepted for interpretation. The geophysical results produce a high reliability of detecting the expected lithology in both sequence and thickness. The DOI index for each model suggests reliability in regions with values less than 0.3, with areas at a higher DOI index representing equivalency problem. The top layers in the 3-D sections for both sites have a lower reliability, but the deeper slices provide accurate results.

Self Potential

We collected self-potential measurements at each site using two saturated lead chloride non-polarizing electrodes with a high impedance voltmeter. The survey utilized the potential amplitude method with the reference electrode fixed at the base station, and the roving electrode moved progressively from station to station. This method allows for a small cumulative error in measurements as well as avoiding the confusion of polarity, allowing for a drift correction to be applied to overcome transient noise (Revil and Jardani, 2013). A total of 253 measurements were taken in-line with ERT and FDEM station locations, with each profile and grid measured as a closed loop. We created a contour map of the distribution of electrical potential at the ground surface relative to the potential at the base station for each site, using the Surfer 10 program by Golden Software. We took drift measurements at the beginning and end of each survey line allowing for a correction for slow drift and electrode polarizations. The first-order linear least-squares separation was applied to the observed field data to separate the residual and regional effect of streaming potentials. The residual data reflects the shallow media where surface water is the dominant source of self-potential measurements, and the regional data reflects the groundwater system, mapping the regional groundwater flow direction.

SP measurements are temperature sensitive and may result in error during in-field measurements. Other sources of noise are transient due to powerlines and telluric sources, which are corrected for in drift corrections. Spatial noise is associated with strong heterogeneity in the near-surface which is filtered out by high-resolution measurements. Revil and Jardani, 2013 suggest utilizing 5 measurements per square meter, but due to the size of grid in survey, the measurements are already high resolution. In field measurements could have been collected by using bentonite mud to lower contact resistance, but we neglected this due to the overlap of other geophysical investigation methods.

Frequency-Domain Electromagnetics

We collected FDEM measurements at each site using the EM-31 ground conductivity meter from Loke, 1995. We took both the vertical dipole mode (VDM) and horizontal dipole mode (HDM) measurements at each station to allow for information at different depths. The intercoil spacing is 3.67 m giving an effective depth of 6 m with VDM and 3 m for HDM. The VDM gives the greatest depth of investigation while HDM is sensitive to shallow structures. A contour map of the apparent conductivity was generated for each site to identify lateral discontinuities in conductive media. The maps were contoured in Surfer 10.

Site-Specific Layout

Site A. Investigations with ERT sounding and in-line SP measurements began in June 2017. Figure 4 displays the configurations for each geophysical method. The two long ERT profiles denoted LLE and LLW are of 30 m length with 21 electrodes at 1.5 m spacing. The short parallel 2-D profiles 1-5 are 15 m in length with 0.75 m electrode spacing and collated into a 3-D inversion model. Each 2-D profile was separated by 2 m in the y-direction. The SP measurements followed all ERT profiles in-line.

In November 2017, we collected FDEM data. The FDEM grid was shifted to be a 10 by 12 m grid with 2 m station spacing. A vertical-dipole and horizontal-dipole mode measurement was made at each station.

Site B. The survey design for site B is shown in Figure 5. We collected three long 2-D ERT profiles, denoted LL1-3, as well as in-line SP and FDEM measurements in November 2017. We designed a 8 by 8 m 2-D grid with 1.5 m station spacing in x and y directions, and SP measurements for each station. The FDEM measurements followed in-line with SP measurements, and vertical and horizontal dipole method was employed at each station. The FDEM grid follows in-line with the SP grid points and the data. We collected the ERT parallel 2-D profiles 1-6 in February of 2018 with 0.5 m x-spacing and 1.5 m y-spacing, allowing for 16 electrodes per line. The 3-D inversion included profiles 1-6 measurements.

Results

<u>Site A</u>

The long profiles, LLE and LLW, of 30 m provided a depth of investigation of 6 m (Figure 6) with an electrode spacing of 1.5 m. This allows for high resolution in vertical sounding due to the spacing being comparable to the top layer sediment thickness. The ERT results from LLE show three electrical layers. The conductive top layer (L1) ranges in resistivity between 70-200 Ωm and 1.5 m thickness, which indicates a media with fine grained electrically conductive top soil layer. This layer is underlain by a resistive layer (L2) interpreted to be sands and gravels, with resistivity between 200-400 Ωm about 3.5 m thickness. We expect the sand and gravel to have a high resistance because the unit is unsaturated and composed of silicate grains which would produce a more resistive response because electrolytic conduction will be dependent on the grain surface and affected by void space in larger pore sizes. The lower geoelectrical layer (L3) produces a low resistivity response less than 100 Ωm, which has been interpreted to be a clay. The response from LLE suggests a horizontal discontinuity among the resistivity layers where the model reflects the basin fill sediment package as expected from well lithology information. However, we found an anomalous high-resistivity response within the sand and gravel layer that lies directly beneath the house. Compared to LLW, this resistive anomaly extends horizontally E-W beneath the house at a depth of 2 m with an unknown total thickness as it extends westward. According to DOI calculations, this anomaly produced a DOI index greater than 0.3 and suggests a problem of equivalency where true values are undetermined (Figure 6). The anomalous response could be due to a buried artifact or a geologic phenomenon, but the source cannot be determined by the scope of our investigation. The response from LLW shows a sharp vertical discontinuity near the anomalous response. To the south end of the line, the resistivity distribution is homogenous with a value of about 90 Ωm. This suggests that there is a geologic discontinuity between the expected sand and gravel at this depth and a fine grained silty-clay composition.

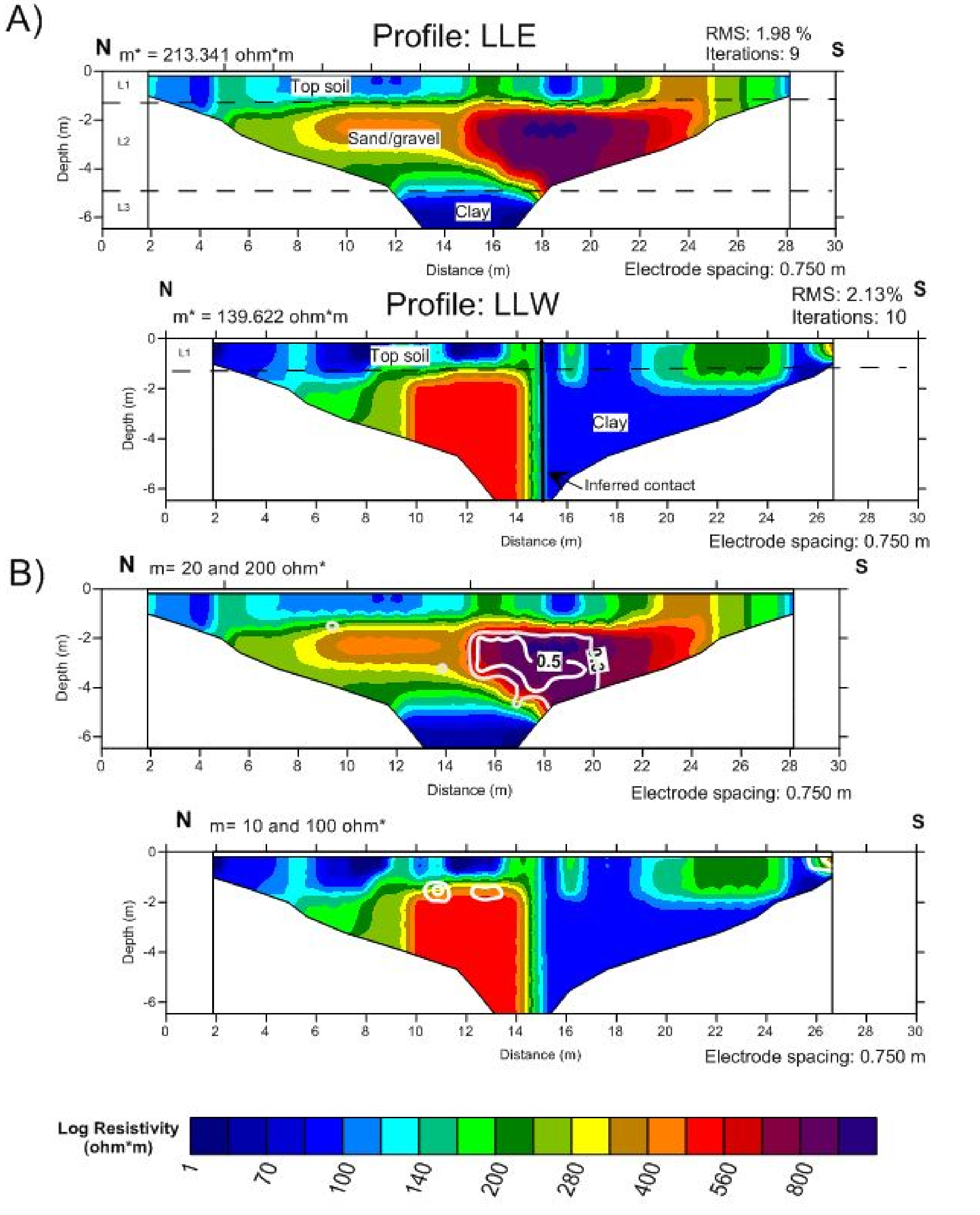

Figure 6 (A) The 2-D ERT models for profiles LLE and LLW are shown. (m*) denotes the background reference resistivity allowed for DOI calculations, shown in (B). DOI values above 0.3 are determined to be unreliable values and are shown in the image.

The 3D resistivity inversion model (Figure 7) shows a maximum depth of 2.2 m and has a high vertical resolution due to 0.75 m electrode spacing from collated parallel 2-D profiles. The known subsidence feature is located at approximately 8 m in the x-direction (W-E) and between 2-4 m in the y-direction (S-N). This feature corresponds with a circular resistive anomaly with resistivity values above 800 Ωm. The subsidence has been filled in with landscaping material and is supposed to produce a resistive response. However, the VOI index shows equivalency error over the circular anomalies presented in the top three slices. The actual resistivity values are not reliable; however, the variation and extent are to be believed. The resistive signature extends to at least 0.4 m depth, with about 1.5 m diameter. We can identify more circular resistive anomalies in this depth range, suggesting the possibility more subsidence features that have failed to collapse, where developing subsurface void space would attribute to high resistivity responses. However, we note the results of this survey cannot definitively confirm this.

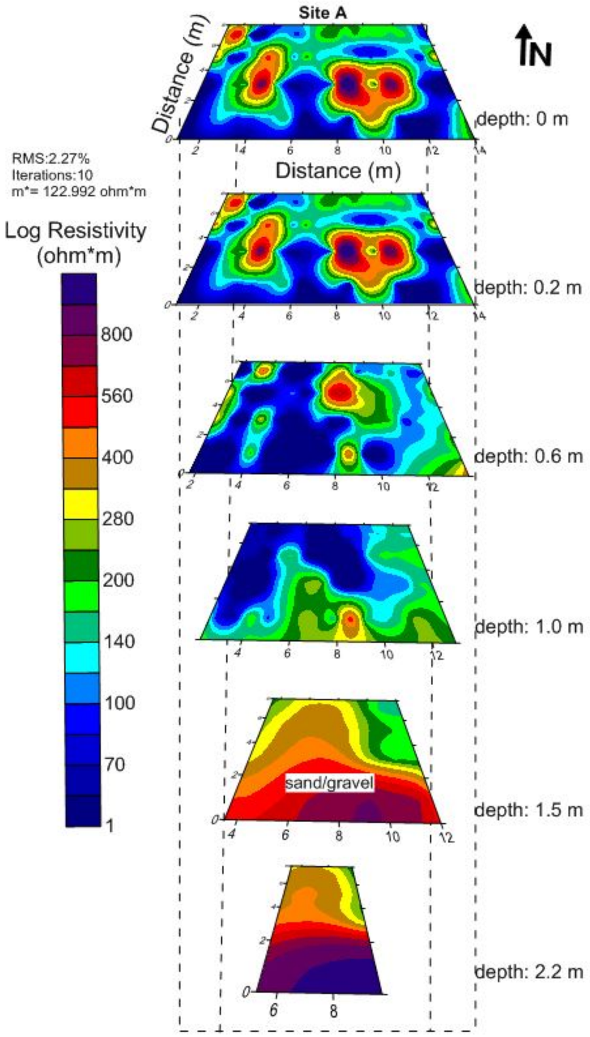

Figure 7 A 3-D resistivity model obtained from inversion of Site A data. The x and y locations are shown. A total of six depth slices are shown to illustrate the lateral apparent resistivity distributions at depth.

The 3-D ERT section provides little data coverage below 1 m depth, but an inferred lithologic contact appears to lie between resistive and conductive media. The FDEM maps (Figure 8) provides greater lateral variation at 3m and 6 m depth, which further illustrates the contact between sediment packages. The HDM response at 3 m presents a very clear contact between resistive sediment, interpreted to be sand and gravel based on the long line results for this package both in depth and high resistivity variation, as well as conductive material with a high clay content. At 6 m depth, the resistive signature is dissipating and suggests that the clay layer does not extend much deeper than 6 m.

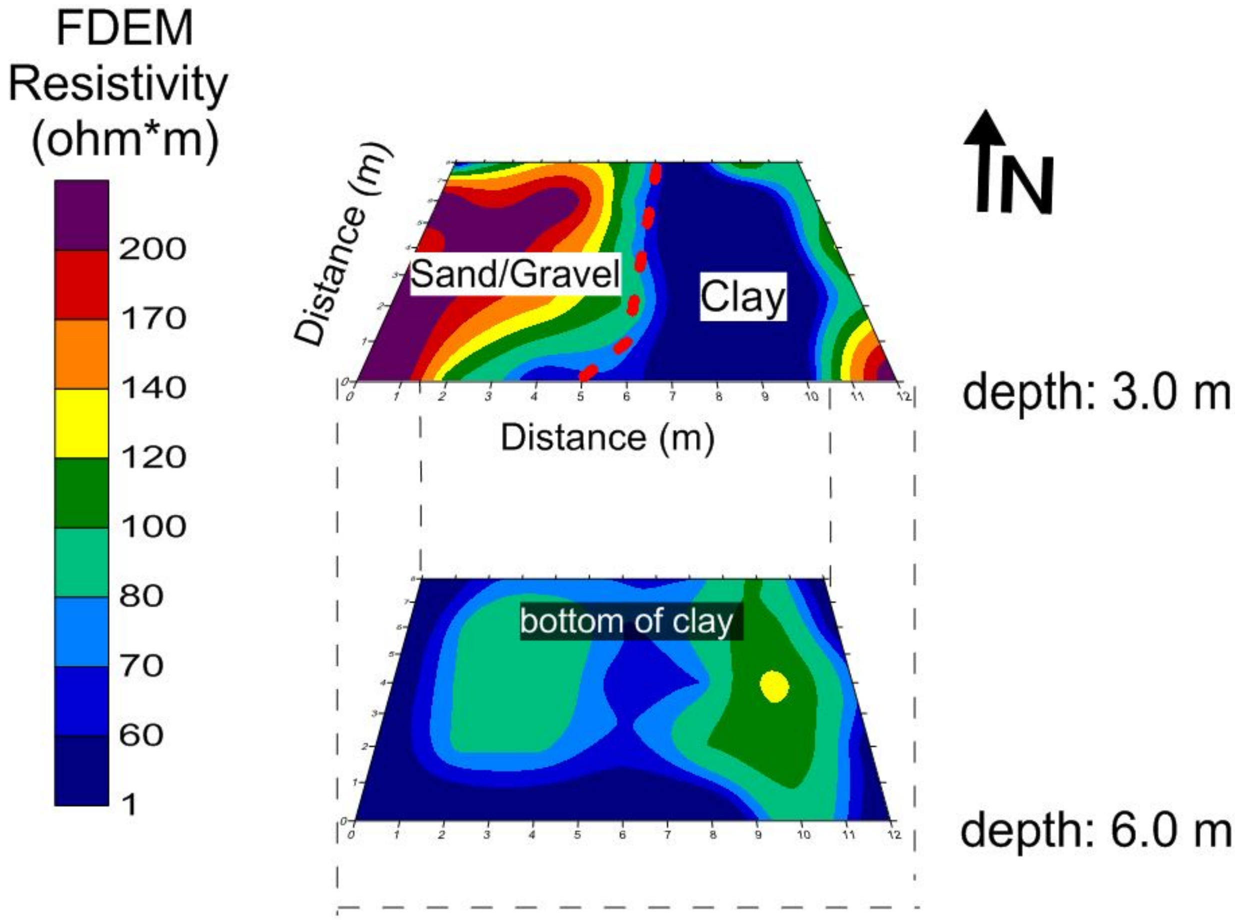

Figure 8 The FDEM contour maps of resistivity is shown. The depths are shown for each grid, with resistivity ranging between 1-200 ohm*m

From the SP results, the residual data show seepage effects in the shallow surface with two negative anomalies with values -34 mV to -16 mV (Figure9). The seepage path is directed from negative recharge zones towards positive values, indicating the infiltration zones (Burke et al, 2011). The subsidence, which has been filled in, is situated in a region with values -1 mV to -4 mV. The positive values on the southern side of the line correspond with the location of the known resistive anomaly. The two positive anomalies on the north side of the grid with values +11 to +17 mV are spatially associated with the negative anomalies. The results indicate there is a flow conduit source that bisects the back yard from E to W, allowing for seepage to be directed to the N and S of the yard. The regional data show the groundwater flow direction is to the NW, which is expected from water table maps from Tucci and Icopini, 2012.

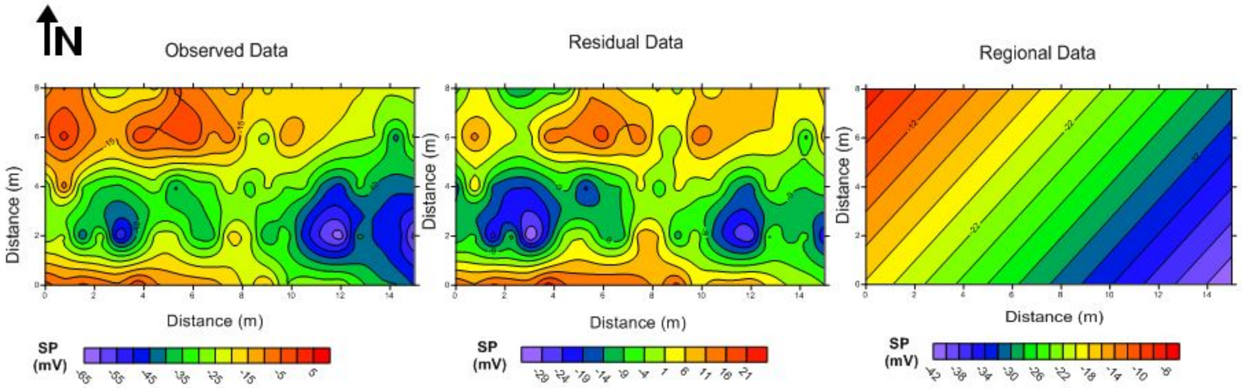

Figure 9 The SP grid for Site A is shown, with the maps generated from a first-order linear least-squares separation. The residual data reflects the shallow surface seepage effect, while regional data reflects the overall groundwater system.

ERT, FDEM, and SP results all show circular resistive anomalies associated with seepage around the subsidence. The seepage anomalies appear to be oriented as a conduit, suggesting an area of recharge. The presence of multiple resistive anomalies along this conduit suggests some correlation between seepage and subsidence occurrence. The FDEM showed a contact in sediments, which lies directly beneath the subsidence feature. This suggests the inhomogeneity in channel fill deposits at 3 m depth as are related to the subsidence occurrence.

<u>Site B</u>

The long profiles for site B, LL1-3, provided a depth of investigation up to 5.5 m, with LL3 being a 20 m length with 4 m depth, and these profiles are shown in Figure 10. Lines LL1 and LL3 intersect and cross at the western side of the property. LL1 is the most expressive as it crosses the subsidence feature at 21 m along the line. The known subsidence location is associated with a resistive anomaly that extends through sands and gravel along the side of the house between 2-4 m depth, although it appears to extend deeper below the scope of the investigation. The profile LL3 also crosses the subsidence feature with a higher resolution of electrode spacing, and this result shows the subsidence feature produces a highly resistive signature greater than 1000 Ωm in the top 0.5 m of the profile, as expected since the feature has been filled with cement. The same anomaly shown in LL1 appears beneath the subsidence, suggesting a horizontal extension at depth of this anomaly. A clear vertical discontinuity lies on the south side of the feature, which shows the heterogeneity between the sand and gravel subsurface and anomalous resistive signature associated with the subsidence. The resistivity values of this anomaly at 300-450 Ωm are associated with the surface location of rain drainage pipes coming off of the roof to the ground surface.

This signature extends around the subsidence feature. The results suggests a surficial seepage response. We note that the surface along the western side of the house is lined with pebbles and cobbles allowing for percolation. However, if looking at the LL2 profile, a similar response is associated with a rain drainage pipe. Yet, the known gardening zone produces a less resistive signature. Beneath the gardening area is a vertical extension between 120-300 Ωm that extends down below 4 m depth. The survey was completed in November, so there is no gardening activity. This may be a cause of the resistivity value differences. This zone may still act as an infiltration zone for the backyard. All three models produce a DOI less than the accepted 0.3, suggesting a high reliability.

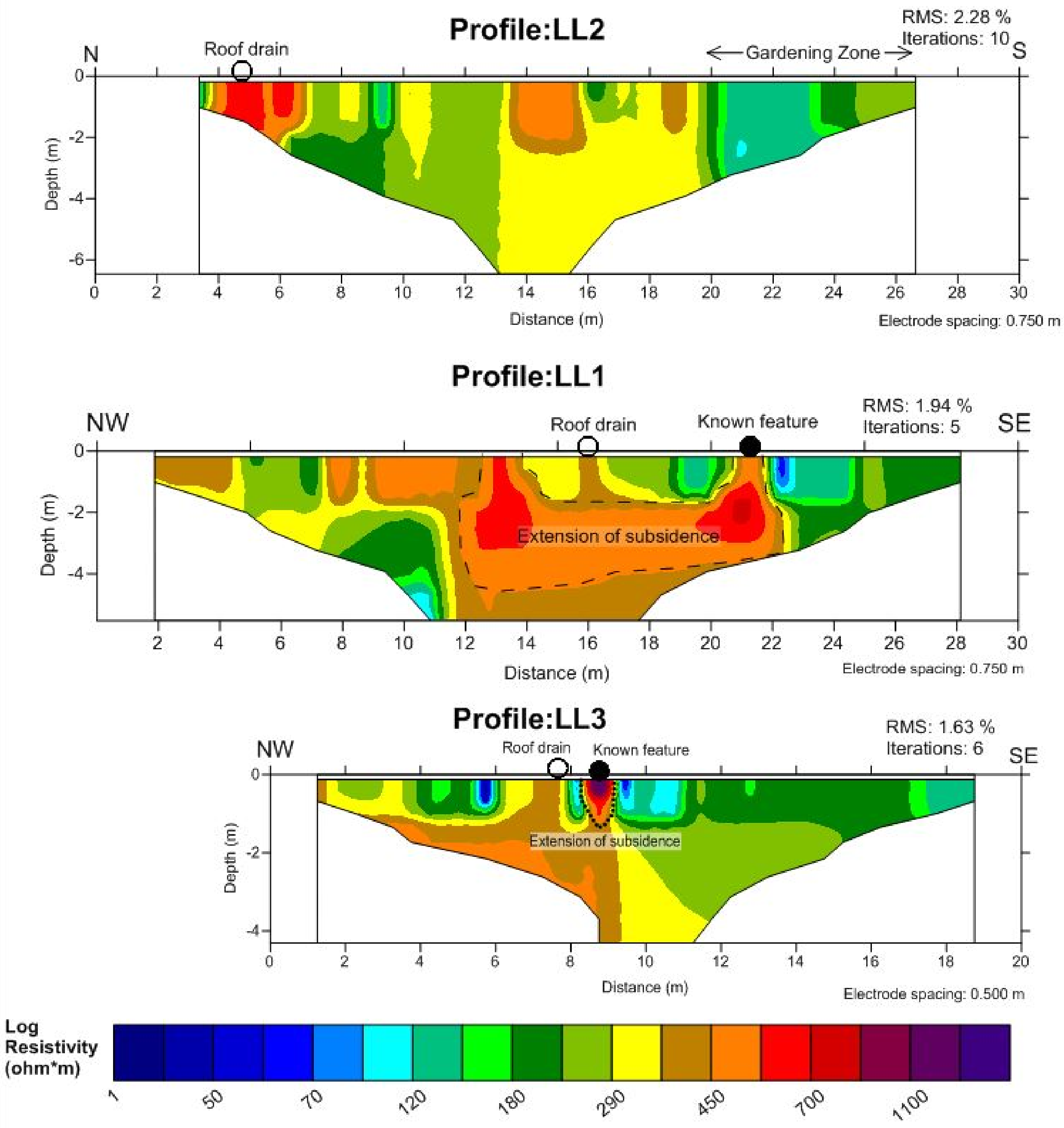

Figure 10 The 2-D long profiles for Site B is shown in alignment with in-field measurements for comparison.

The 3-D resistivity inversion model (Figure 11) shows a maximum depth of 1.5 m and has a high vertical resolution due to 0.50 m electrode spacing from collated parallel 2-D profiles. The known subsidence feature is located at approximately 0 m in the x-direction (W-E) and between 7-8 m in the y-direction (S-N). This feature corresponds with a circular resistive anomaly with resistivity values above

2500 Ωm, but the feature is better expressed in the 2-D profiles. We note that the 3-D model data reflects results from February; thus, the resistivity values will differ. However, the VOI index shows equivalency error over the circular anomalies presented in the top three slices. The actual resistivity values are not reliable; however, the variation and extent are to be believed. The resistive signature extends to at least 0.4 m depth, with about 1.5 m diameter in each anomaly. More circular resistive anomalies are present in this depth range, suggesting potential subsidence features that have failed to collapse. However, we cannot definitively assume this. The 3-D results are limited at depth, but the model shows an apparent contact between resistive and conductive sediments. This contact is associated with the trend of anomalies seen in the top three slices.

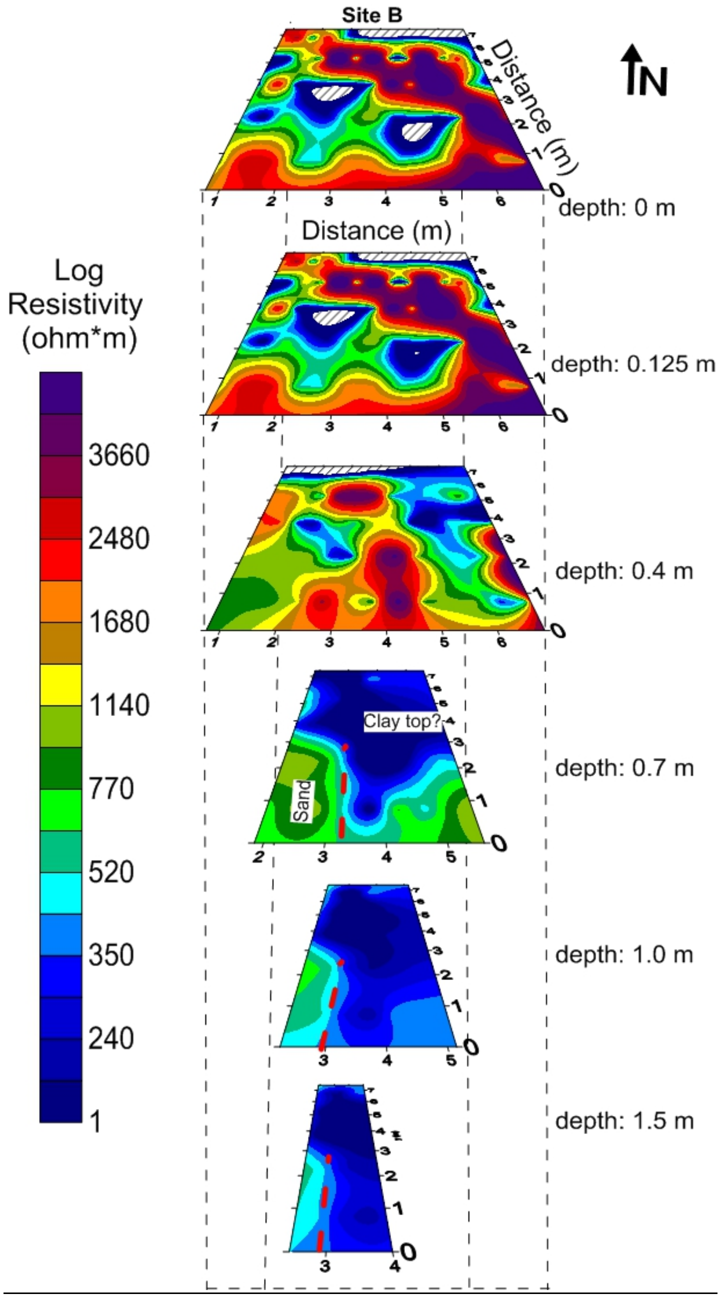

Figure 11. A 3-D resistivity model obtained from inversion of Site B data parallel 2-D data. The x and y locations are shown. A total of six depth slices are shown to illustrate the lateral apparent resistivity distributions at depth. The hatched reasons are areas with no model information.

The FDEM further enhances the subsurface model from the ERT results. The HDM and VDM results shown in Figure 12 at 3 m and 6 m express the contact between resistive and conductive material. The HDM results clearly demonstrate a contact between sand and gravel with clay, which is known to exist at this depth due to lithologic information from GWIC wells. The contact follows the trend of the surface anomaly features. The VDM results show the clay layer dissipating.

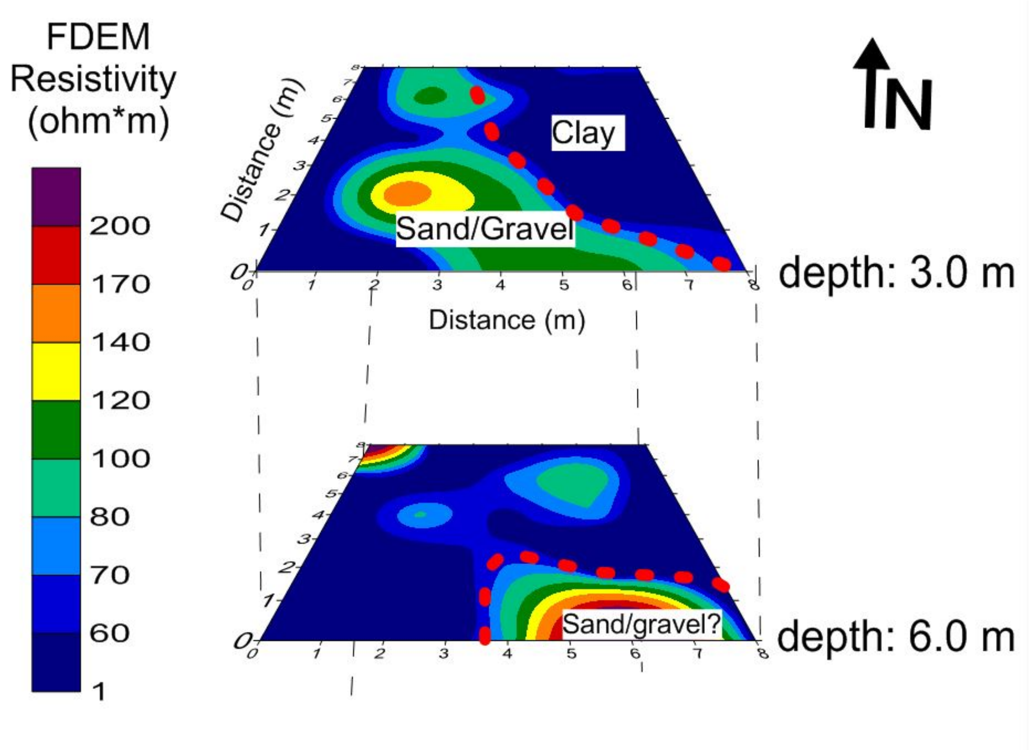

Figure 12. The FDEM map for Site B is shown for HDM (3 m) and VDM (6 m) measurements. A contact between sand and gravel with clay is shown clearly at 3 m depth and dissipates at 6 m depth.

The SP results (Figure 13) provide some information about the seepage patterns occurring in the grid of the backyard. The residual data shows a clear surficial seepage zone coming from the SE corner of the yard and extending NW towards the subsidence feature as well as other surface anomalies. We identify a seepage zone along the western edge of the yard, with an anomaly associated by the subsidence feature. The seepage zone is also associated with the resistive distribution shown in the lower ERT slices and FDEM results. The regional data corresponds with results from site A with general groundwater flow trending to the NW towards the Silver Bow Creek and Berkeley Pit (Figure 1).

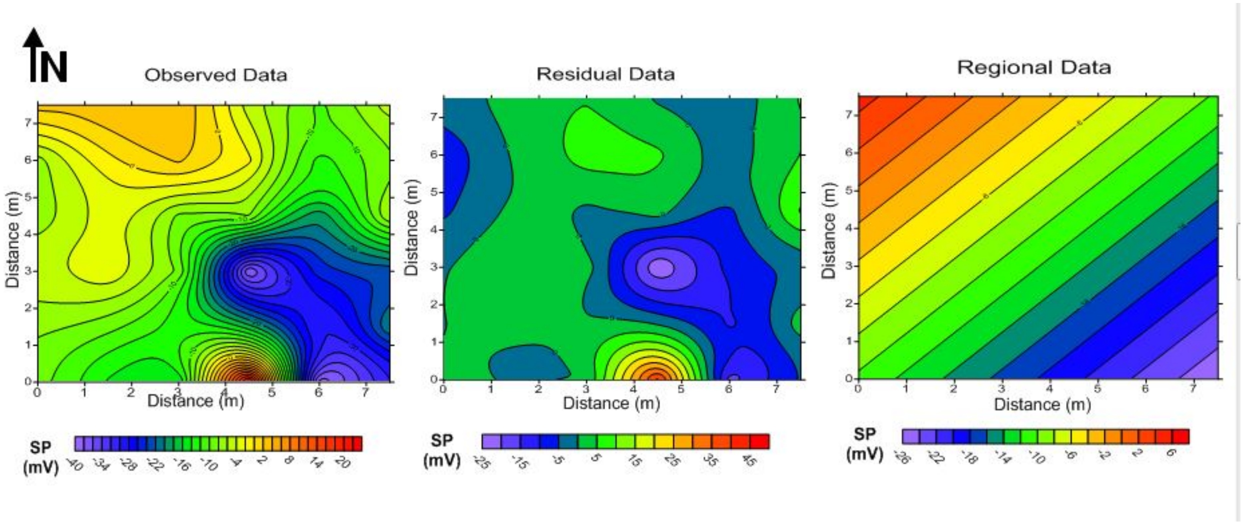

Figure 13. The contour map of SP field measurements, with a first-order linear least-squares separation technique. The residual data reflects the shallow surface seepage effect, with regional reflecting the overall groundwater system.

Geological Cross-Sections

We developed two geological cross-sections to illustrate the lithologic information obtained from well logs. The geophysical data covers in high-resolution the site-specific lithologic structure in each yard, but the geologic information provides an illustration on the regional distribution. Since the geophysical investigation only reaches a depth of 6 meters, only the vadose zone within the geologic cross-sections is considered.

The cross section lines AA’ and BB’ and GWIC wells are shown in Figure 1. In cross section AA’ (Figure 14a) includes seven GWIC wells. Well 150413 is located in between the geophysical investigation sites, allowing for information to apply to both sites. Beneath the silty and organic top soil layer lies a coarse sediment layer of sand and gravel. A clay layer appears to be a lens in the E-W direction, with the well log describing this clay lens as a clay that “balls easily”, indicating a high clay content. The clay lens is underlain with fine sand, which acts as an aquifer unit for the shallow aquifer, with water levels defined in GWIC well lithology information. The red triangles represent nearby subsidence features that lie within a couple hundred meters from the cross-sectional line. Most features are associated with the clay lens found at approximately 3 m depth. Well 224152 describes the shallow layer as a silty clay, which is still in contrast to the overlying and underlying sediment. Cross section BB’ (figure 14b) shows similar sediment distribution as AA’, but the clay lens extends as a layer in the NE-SW direction. The same well 150413 with sites A and B is in the cross-section, but two other sites lie along this line. The clay layer lies within the vadose zone, with a porous media above and below the layer. The unity of this sediment package amongst multiple sites of subsidence suggest a common cause is associated with the lithologic structure within this vadose zone.

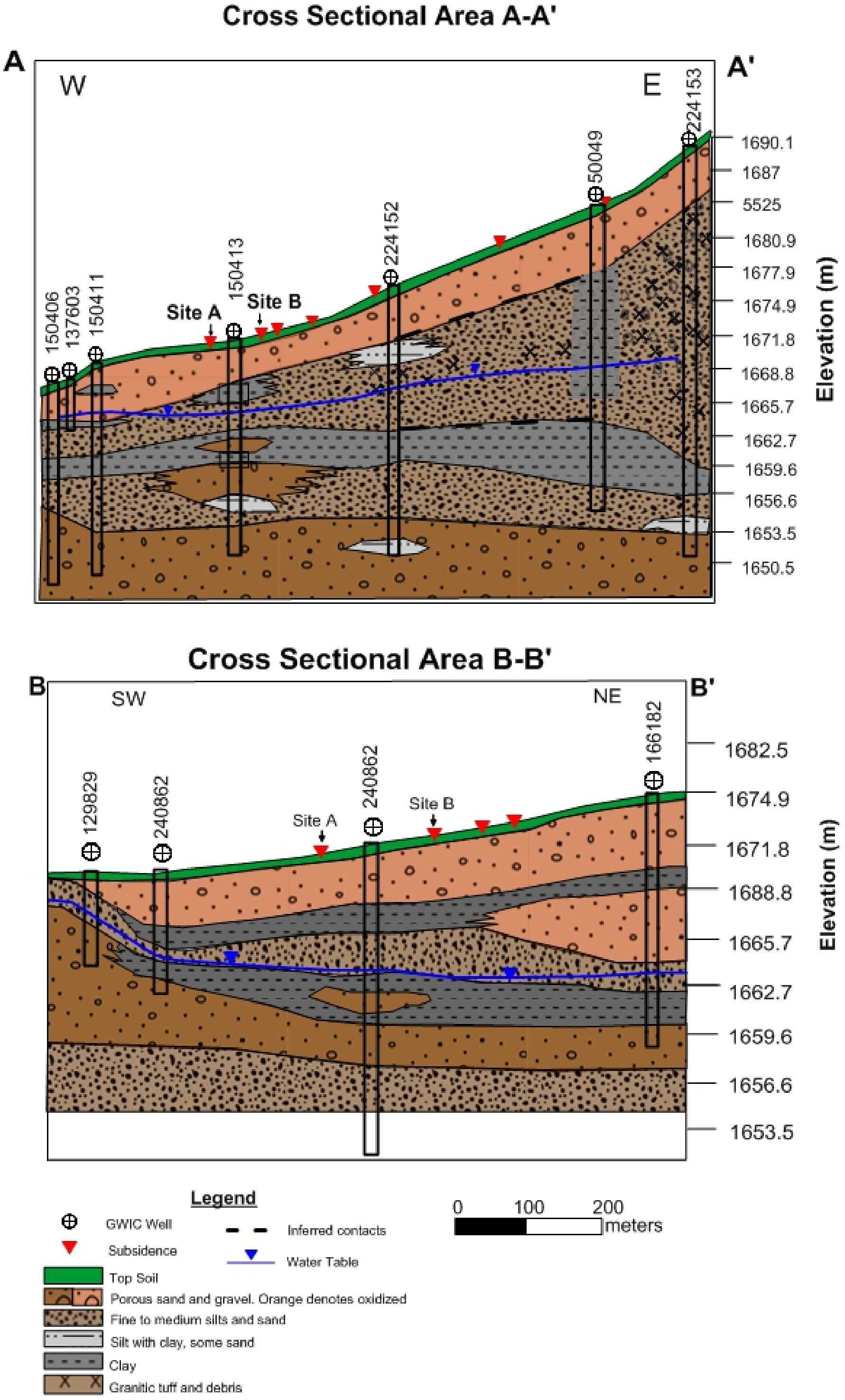

Figure 11 a) The hydrogeologic cross sections A-A' and b) B-B' generated with borehole information (Montana Groundwater Information Center Water Well Data, 2012)

Lithology and Geo-electric layers. Based on the hydrogeologic and geologic information of the study area, the resistivity and FDEM sections illustrate three geoelectric layers within the vadose zone. The layers include:

1. Middle resistivity silty loam and organic top layer
2. High resistivity dry sand and gravel layer
3. Low resistivity clay layer

The layers have been confirmed through comparisons with well lithologic information from 150413, as well as the geologic cross-sections generated from multiple well lithologies. Figure 15 shows the correlation for both sites with the known lithology. The clay layer is expressed in both sites, with a similar vertical extension of the clay layer from 3-6 m. However, site B appears to have higher clay content at a shallower depth, as determined by the homogenous conductivity variation compared between both sites. This corresponds well with geologic cross-section, where site B lies at a higher elevation. The clay layer disappears at 6 m depth for both sites.

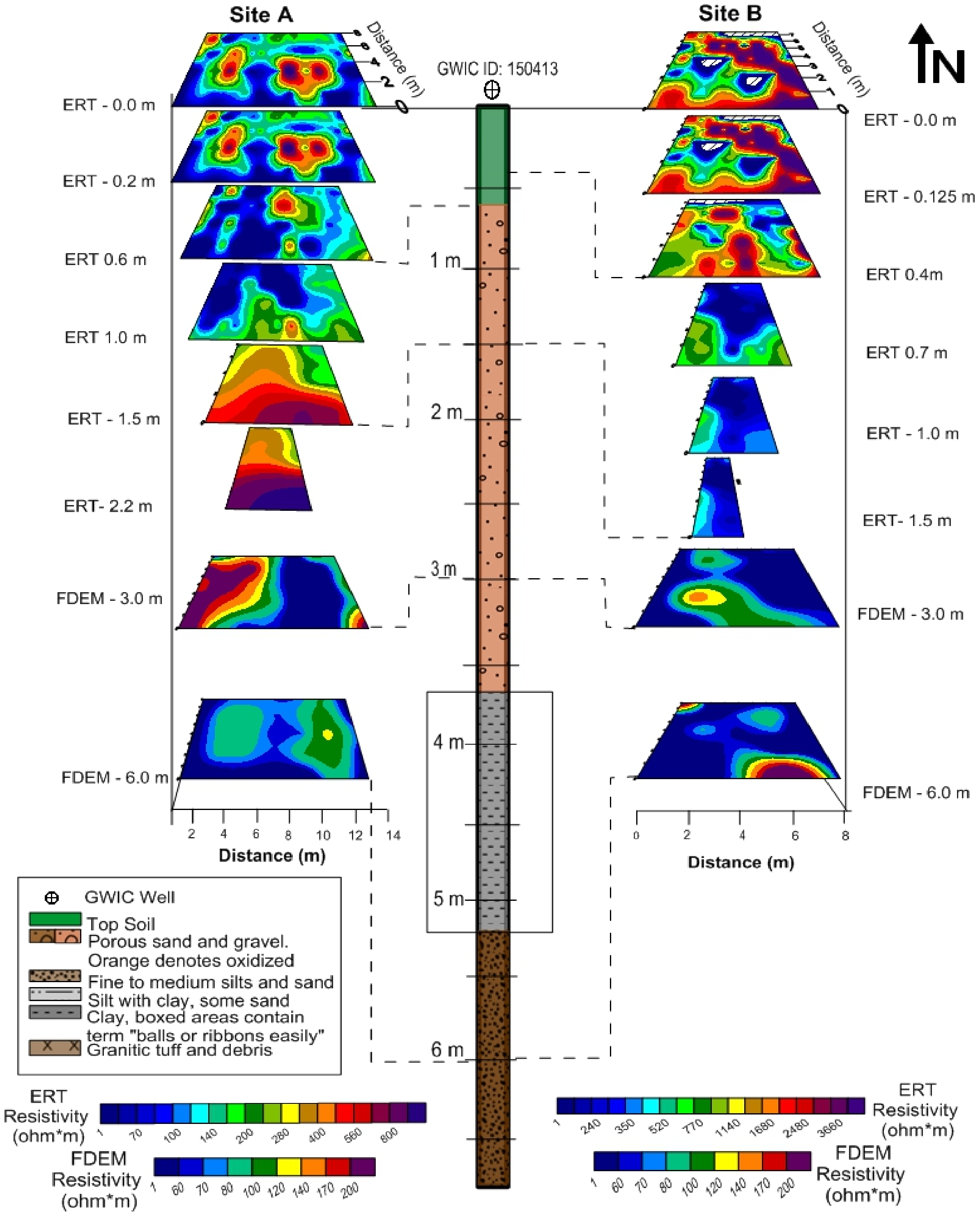

Figure 15. The 3-D inversion models compared with well log lithology from GWIC well 150413. The well is located 120 m NE of Site A and 150 m SW of Site B. The horizontal scale is not depicted in the figure. Depths for ERT slices and sediment layers are shown

Discussion

The shallow geophysical models of the subsidence features in this study have identified the combination of a shallow clay lens below the subsidence feature and surficial seepage anomalies associated with each feature. The results suggest that clay and surficial seepage provide favorable conditions for subsidence.

The driving mechanism leading to subsidence is believed to be of natural origin, which may include one or a combination of the four main processes of subsidence as mentioned in de Glopper and Ritzema, 1994. Clay is known to be associated with subsidence mechanisms in a variety of scenarios, including non-seismic liquefaction (Tuttle, 2001, Holzer and Clark, 1993) and artificial recharge (Zhang et al., 2015); however, these scenarios do not consider the effect of surficial seepage. The combination of surficial seepage and clay can be explained with the concepts of hydrocompaction or swelling of soils.

Clays are known to correlate with subsidence, depending on the amount, type, and moisture content of the clay (Bull, 1964, Liu et al., 2000) where soft clays in shallow layers are known to have a higher subsidence potential (de Glopper and Ritzema, 1994). A smectite clay is derived from volcanic ash or tuff and has a high swelling potential, especially if consisting of montmorillonite (Liu et al., 2000, Bull, 1964, de Glopper and Ritzema, 1994). The alluvial deposits in the Silver Bow alluvial basin are derived from Butte Quartz Monzonite (BQM), in which a common alteration will produce montmorillonite and other smectite clays (Zhang, 2000). We believe that the shallow clay lens found in both sites may have a high swelling potential.

According to de Glopper and Ritzema, 1994, compaction and consolidation are processes associated with clay and subsidence. In particular hydrocompaction is a process of collapse and compaction of soils in silty to sandy sediment associated with the presence of clay. As surface water infiltrates overlying porous sediments, the interparticle bonds between clay and coarse grains is broken and reduces the capillary tension established when unsaturated. The removal of structural bonds causes a consolidation of sediments manifested by ground subsidence (Bull, 1964, Zisman and West, 2015, de Glopper and Ritzema, 1994). The subsidence in both sites is occurring within the porous layer in the top 2 m of subsurface, in which gradual and cyclical hydrocompaction could be taking place. According to Zisman and West, 2015, void spaces will develop in the subsurface under a void roof. If large void spaces are forming in the sites, they would produce a larger resistivity response, and this condition may attribute the the new circular resistive anomalies found in both sites. A similar phenomenon is described in Liu and Li, 2005, and they suggest that smectitic clays may undergo primary consolidation and secondary compression. This process occurs within the clay lens itself, where primary consolidation gradually releases excess pore-water and increases stress, while secondary compression relates to clay dehydration (Liu and Li, 2005, Liu et al, 2000). This dehydration process involves the release of interlayer water and can result in up to 36.3% volume reduction in smectitic clays (Liu et al., 2000). As a consequence, we suspect that clay contributes to volume reduction at the sites.

Both hydrocompaction and clay dehydration are gradual processes, where the cyclical swelling and dehydrating of clay will cause repeated cycles of tension over time (Bull, 1994, Liu and Li, 2005). The swelling and dehydrating of clay would occur with seasonal moisture cycles, where there may be 3-5 months of rain and 7-9 months of little to no rain which will remove moisture from surface deposits (Bull 1964). We note that we do not know the specific dates of subsidence occurrence for all sites in this survey, but we suggest that seasonal cycles contribute to the gradual development of subsidence over the past eighty years. If cyclical swelling and shrinking of the clay is a dominant process for the Silver Bow alluvial basin, the triggering mechanism would lie in the explanation of surficial seepage. The addition of infiltrating surface water will cause compaction to increase suddenly, causing a rapid change in strength and soil particles to move downward due to erosion (Bull, 1964, Zisman and West, 2015). In this type of environment, structures that do not have proper gutters and drainage pipes to direct water away from the building is more susceptible to collapse and settle (Zisman and West, 2015). In Site A, the excessive watering of the yard would have followed the natural seepage paths defined in SP results and further contributed to surface water infiltration In Site B, the improper installation of rain gutters onto percolating gravels would also contribute the natural seepage paths of the yard. Due to the knowledge of excessive watering, the association of drainage pipes near the subsidence features, and evidence of structural damage, surface water infiltration appears to have a connection to subsidence occurrence.

The geophysical evidence from this study provides analysis on the shallow subsurface below 6 m, to which we suggest some conclusions on the local mechanisms contributing to each subsidence feature. We suggest further investigation to either accept or reject the possibilities of regional causes such as liquefaction and artificial recharge. So far there has been no evidence of vertical extension of subsidence feature anomalies into the deeper subsurface or to a large fissure, as suggested in both seismic and non-seismic liquefaction subsidence origins. A large fissure would be a strong indication of liquefaction as it acts as a hydraulic connection between the subsidence sites (Holzer and Clark, 1993). In Wolf et al, 1998, liquefaction features may be overshadowed by sediment facies, but further investigation would be needed regionally to identify a trend between the subsidence features. Artificial recharge is also a possible mechanism for subsidence; however, the geophysical evidence in this study focuses only on two sites. Artificial recharge will require a regional investigation of land elevation changes with time, to which the shallow clay layer found in the borehole and geophysical information may have a contribution to the location of subsiding features. We suggest further geophysical investigation into the deeper subsurface, to include more sites, and to utilize induced polartization techniques (IP) to map the true extent of the clay layer and its association with the subsidence features. We also recommend on-site drilling and soil sampling to identify the true clay swelling potential. Lastly, many common mechanisms of subsidence are associated with a regional land subsidence, so information may need to be collected on regional ground elevation changes.

Conclusions

The susidence features of this study are characterized by instantaneously forming circular depressions in the shallow subsurface with no connection to buried artifacts or structural voids. The features located within the Silver Bow Creek alluvial basin show a spatial correlation to surface water seepage paths, sharp contacts between sand and clay material, and direction of groundwater flow. The resistivity sections identify sedimentary layers with known depths and thicknesses from well-logs as well as identify subsidence features. ERT and FDEM methods join to form lateral and vertical variations of resistivity with a depth to 6 m. The self-potential maps support electrical resistivity and electromagnetic conduction results by mapping groundwater flow along sedimentary material discontinuity. This study has accurately delineated the lithologic features in thickness and depth in residential properties that have experienced subsidence. The reported subsidence features produce a resistive circular response, spatially associated with seepage patterns. The results suggest the presence of clay in the vadose zone contributes regional occurrences of subsidence as surface water infiltrates the porous overlying sand and gravel layer. The mechanisms of hydrocompaction and saturation of the clay layer is believed to contribute to the vertical displacement of sediments. Within the scope of this investigation, we suggest the favorable condition that promotes subsidence is related to shallow clay and sand heterogeneity experiencing cyclical seepage events attributed to both seasonal changes and man-made activity.

Acknowledgements

This research was supported by the Geophysical Engineering Department of Montana Tech. We thank the City and County of Butte Silver Bow for access to sites and hazard information. We also wish to thank the Butte residents for their permission to conduct data collection on their properties.

References

Bezerra, F.H.R, Da Fonseca, V. P., Vita-Finzi, C., Lima-Filho,F.P., and Saadi,A., 2005, Liquefaction-induced structures in Quaternary alluvial gravels and gravelly sediments, NE Brazil: Engineering Geology, **76** (3),191-208.

Bozeman, M.T., 2002, Underground hard-rock mining: subsidence and hydrologic environmental impacts.

Bull, W.B., 1964, Alluvial fans and near-surface subsidence in Western Fresno County California: *in* Studies of Land Subsidence, Department of Water Resources, and Geological Survey, Issuing Body.

Burke J.M., Burton, B.L., Ikard, S., and Powers, M.H., 2011, Hydrogeophysical Investigations at Hidden Dam, Raymond, California: Journal of Environmental & Engineering Geophysics, **16** (4), 145-164.

De Glopper, R.J., and Ritzema, H.P., 1994, Land subsidence: *in* Drainage Principles and Applications, ILRI, **16** (2), 417-512

Doolittle, J.A., Indorante, S.J., Potter, D.K., Hefner, S.G., and McCauley, W.M., 2002, Comparing three geophysical tools for locating sand blows in alluvial soils of southeast Missouri*:* Journal of Soil and Water Conservation, **57** (3), 175-182.

Gammons, C., Metesh, H., and Duaime, J., 2006, An Overview of the Mining History and Geology of Butte, Montana: Mine Water and the Environment, **25** (2), 70-75.

Holzer, T., and Clark, M. 1993, Sand boils without earthquakes: Geology, **21** (10), 873.

Houston, Andrew R., 2001, Geology and structural history of the Butte district, Montana: M.Sc. thesis. Oregon State University, Corvallis, Oregon.

Jardani, A., Revil, A., Akoa, F., Schmutz, M., Florsch, N., and Dupont, J.P., 2006, Least squares inversion of self-potential (SP) data and application to the shallow flow of ground water in sinkholes: Geophysical Research Letters, **33** (19).

Liu, C.W., Lin, W.S., Shang, C., and Liu, S.H., 2000. The effect of clay dehydration on land subsidence in the Yun-Lin coastal area, Taiwan: Environmental Geology, **40** (4-5), 518-527.

Loke, M.H., 1996, Rapid 2D Resisitivty & IP Inversion using the least-squares method: *in* Geotomo Software Manual.

Loke, M.H., 2004. Tutorial: 2-D and 3-D electrical imaging surveys: *in* Geotomo Software, Malaysia.

McDonald C., Elliot, C.G., Vuke, S.M, Lonn, J.D., and Berg, R.B., 2012, Geologic Map of the Butte South 30’ x 60’ Quadrangel Southwestern Montana: in Open File Report, Montana Bureau of Mines and Geology, 622.

Newbrough, P., and Gammons, C., 2002, An experimental study of water–rock interaction and acid rock drainage in the Butte mining district: Montana. Environmental Geology, **41**(6), 705-719.

Obermeier, S.F., 1996, Use of liquefaction-induced features for paleoseismic analysis – an overview of how seismic liquefaction features can be distinguished from other features and how their regional distribution and properties of source sediment can be used to infer the location and strength of Holocene paleo-earthquakes: Engineering Geology, **4** (1-4), pp.1-76.

Oldenburg, D.W., and Li, Y., 1999, Estimating depth of investigation in dc resistivity and IP surveys: Geophysics, **64** (2), 403-416.

Revil, A., and Jardani, A., 2013, The self-potential method: Theory and applications in environmental geosciences: Cambridge University Press, New York, 1-14, 160-167.

Reynolds, J.M., 2011, An introduction to applied and environmental geophysics, 2nd ed.: John Wiley & Sons, Chichester.

Soupios, P.M., Georgakopoulos, P., Papadopoulos, N., Saltas, V., Andreadakis, A., Valliantos, F., Sarris, A., and Makris, J. P., 2007, Use of engineering geophysics to investigate a site for a building foundation: Journal of Geophysics and Engineering, **4**(1), p.94.

Stumpf, A.J., 2013, Collapsing Soil Hazards: in Bobrowsky P.T. (Eds) Encyclopedia of Natural Hazards. Encyclopedia of Earth Sciences Series, Springer, Dordrecht.

Tuttle, M., 2001, The use of liquefaction features in paleoseismology: Lessons learned in the New Madrid seismic zone, central United States: Journal of Seismology, **5**(3), 361-380.

Tucci, N.J., and Icopini, G.A., 2012, Geochemical and Hydrogeologic Investigation of Groundwater Impacted by Wastes Left in Place in the Butte Priority Soils operable Unit Butte, MT: *in* Open File Report 613, Montana Bureau of Mines and Geology.

Tucci, N.J., 2010, The Parrot complex: A drilling investigation of historic mine waste left in place; tailings and overburden volumes, leachability and economic feasibility for recovery, and water quality along the upper Metro Storm Drain in Butte, Montana: *in* Open File Report 590, Montana Bureau of Mines and Geology, 46.

United States Department of Agriculture, Natural Resources Conservation Service, 2009, Soil Survey of Silver Bow County Area and Parts of Beaverhead and Jefferson Counties, Montana.

Wolf, L.W., Collier, J.,Tuttle, M., and Bodin, P., 1998, Geophysical reconnaissance of earthquake-induced liquefaction features in the New Madrid seismic zone: Journal of Applied Geophysics, **39**(3), 121-129.

Zhang, Y., Wu, J., Xue, Y., Wang, Z., Yao, Y., Yan, X., and Wang, H., 2015, Land subsidence and uplift due to long-term groundwater extraction and artificial recharge in Shanghai, China: Hydrogeology Journal, **23**(8), 1851-1866.

Zhang, L., 2000, Stable isotope investigation of a hydrothermal alteration system: Butte porphyry copper deposit: PhD. thesis, Oregon State University, Corvallis, Oregon.

Zisman, E., and West, S., 2015, Hydrocompaction Considerations in Sinkhole Investigations: *in* National Cave and Karst Research Institute 5th Symposium, University of South Florida.

http://data.mbmg.mtech.edu/mapper/mapper.asp?view=Wells& accessed on 06/15/2018.

http://mbmggwic.mtech.edu/ accessed on 07/17/2018.